A backwards-tracking Lagrangian-Eulerian method for viscoelastic free surface flow simulation

Simon Ingelsten[1,2], Roland Kádár[2], Andreas Mark[1] and Fredrik Edelvik[1]
[1] Fraunhofer-Chalmers Research Centre for Industrial Mathematics, 412 88 Gothenburg, Sweden
[2] Division of Engineering Materials, Department of Industrial and Materials Science, Chalmers University of Technology, Gothenburg SE-412 96, Sweden

ABSTRACT

A new numerical method for simulation of viscoelastic fluid flow is proposed, based on a previously developed Lagrangian-Eulerian. The viscoelastic constitutive equation is solved in Lagrangian nodes with a backwards-tracking procedure and the fluid momentum and continuity equations are discretized with the finite volume method on an adaptive octree grid. Two-fluid flow is modeled with the Volume of Fluid method.

The new method improves both the robustness and computational efficiency in comparison to the original method. A validation is performed for a viscoelastic planar Poiseuille flow, as well as for simulation of industrial scale adhesive application on an automotive part. The results are in good agreement with available analytic and experimental data. The results also demonstrate the robustness of the numerical framework for simulating complex, industrial scale viscoelastic flows.

INTRODUCTION

Many industrial applications involve viscoelastic fluid flow. Examples include additive manufacturing, polymer extrusion as well as different hybrid joining operations with adhesives. The latter has gained attention partly due to an increased demand for lightweight products, which may require new combinations of materials in for example automotive manufacturing.

Due to the complex nature of viscoelastic flows, different numerical approaches have been proposed over the years. Many examples of them use Eulerian discretization with finite volumes[8,13,14] or finite elements[6,16]. In addition, some type of stabilization method is often used to avoid the numerical instabilities commonly referred to as the High Weissenberg Number Problem (HWNP)[12]. There exist both simple approaches such as both-sides diffusion (BSD) and more advanced methods as the Log-Conformation Representation (LCR)[15,17] or the Square-Root Conformation Representation (SRCR)[20].

An alternative approach is to solve the viscoelastic equations in the Lagrangian frame of reference. A motivation for this is to avoid numerical diffusion in the constitutive equation, which typically does not involve a physical diffusion term. One example is the Lagrangian finite element method by Rasmussen and Hassager[4], in which the entire flow history was stored and re-meshing was required throughout the simulation. Another is the split Lagrangian-Eulerian method for viscoelastic Stokes flow by Harlen et al.[5] where the constitutive equation was solved at the nodes of a co-deforming mesh and the velocity and pressure fields were solved with a Eulerian finite element method. Also in their method, re-meshing was required as the mesh became distorted. The Lagrangian Particle Method (LPM) was proposed by Halin et al.[7] in which the constitutive equation was integrated along the trajectories of massless particles. Polynomial expressions were fitted to the stresses and was included in a Eulerian finite element method. A minimum of three particles per two-dimensional element was required to fit the polynomial expressions. The method was further developed to an adaptive version,

denoted ALPM[9], and to a backwards-tracking version, denoted BLPM[11], in which the particles were tracked backwards in time such that their final location always was known a priori.

In previous research, a Lagrangian-Eulerian method for viscoelastic fluid flow has been proposed and validated,[28] as well as evaluated in terms of computational efficiency.[29] In the method, the viscoelastic constitutive equations are solved in Lagrangian nodes which are convected by the flow. The fluid momentum and continuity equations are discretized with a Eulerian finite volume method.

In this paper, the method is further developed to a backwards-tracking method, where the solution of the constitutive equation is partly inspired by the BLPM method of Wapperom et al.[11] The new method increases the robustness as well as reduces the computational cost of the Lagrangian-Eulerian method. The method is implemented in the flow solver IPS IBOFlow®[1], developed at the Fraunhofer-Chalmers Centre in Gothenburg, Sweden. The solver utilizes the mirroring immersed boundary method[18,19] and an automatically generated and adaptively refined Cartesian octree mesh. Prior to this work, the solver has been employed for numerical simulation of conjugated heat transfer[21], fluid-structure interaction[23] and of two-phase flows of shear-thinning fluids such as seam sealing[22,26], adhesive application[24] and 3D-bioprinting[27].

The paper is structured as follows. First the numerical method is presented, and the differences compared to the original method are highlighted. A validation for a planar Poiseuille flow is then presented, followed by a simulation of industrial scale adhesive application onto an automotive part for which the results are compared to a 3D-scanned experimental adhesive bead.

GOVERNING EQUATIONS

Viscoelastic flow is modeled by the incompressible momentum and continuity equations,

$$\rho\frac{\partial \mathbf{u}}{\partial t}+\rho\mathbf{u}\cdot\nabla\mathbf{u}=-\nabla p+\nabla\cdot(2\mu\mathbf{S}+\tau)+\mathbf{f}, \quad (1)$$

$$\nabla\cdot\mathbf{u}=0, \quad (2)$$

where $\mathbf{u}$ is velocity, ρ density, p pressure, μ solvent viscosity, i.e. the Newtonian contribution to viscosity, $\mathbf{S}$ the strain rate tensor, τ the viscoelastic stress tensor and $\mathbf{f}$ body force. The strain rate tensor is the symmetric part of the velocity gradient $\nabla\mathbf{u}$,

$$\mathbf{S}=\frac{1}{2}\left(\nabla\mathbf{u}+(\nabla\mathbf{u})^T\right). \quad (3)$$

The evolution of the viscoelastic stress is described by a constitutive equation. In this work the exponential form of the Phan Thien Tanner (PTT) model[2] is used, for which the constitutive equation reads

$$\lambda\overset{\triangledown}{\tau}+\exp\left(\frac{\varepsilon\lambda}{\eta}\mathrm{Tr}(\tau)\right)\tau=2\eta\mathbf{S}, \quad (4)$$

where λ is relaxation time, η polymeric viscosity, ε a model parameter and $\mathrm{Tr}(\tau)$ the trace of τ, i.e. the sum of its normal components. The entity $\overset{\triangledown}{\tau}$ is called the upper-convected derivative of τ and reads

$$\overset{\triangledown}{\tau}=\frac{D\tau}{Dt}-(\nabla\mathbf{u})^T\cdot\tau-\tau\cdot\nabla\mathbf{u}, \quad (5)$$

where $D\tau/Dt$ is the Lagrangian, or material, time derivative of τ.
Furthermore, a multimode approach is considered, such that the total viscoelastic stress is the sum of stresses corresponding to the respective N relaxation modes, as

$$\tau=\sum_{k=1}^{N}\tau_k. \quad (6)$$

Each tensor τ_k is then described by an equation of the form of Equation (4) with its own set of parameters $(\lambda_k,\eta_k,\varepsilon_k)$.

Free-surface flow is modeled with the Volume of Fluid (VOF) method. The respective fluid phases are locally represented by the volume fraction $\alpha\in[0,1]$, described by the transport equation

$$\frac{\partial\alpha}{\partial t}+\mathbf{u}\cdot\nabla\alpha=0. \quad (7)$$

For $\alpha = 1$ only phase 1 is present, for $\alpha = 0$ only phase 2 is present and for $\alpha \in (0,1)$ there is a mixture, implying an interface between the two phases. Local fluid properties ϕ, e.g. as density or viscosity, are defined as the average

$$\phi = \alpha\phi_1 + (1-\alpha)\phi_2, \tag{8}$$

where ϕ_1 and ϕ_2 are the properties the respective phases.

NUMERICAL METHOD

The numerical method presented in this work is based on the Lagrangian-Eulerian framework for viscoelastic flow proposed by Ingelsten et al.[28,29] The momentum and continuity equations, as well as the transport equation for α, are discretized with a collocated finite volume method on a Eulerian octree grid and solved with the SIMPLEC method[3]. Equation (7) for α is discretized with the shock-capturing CICSAM scheme[10], designed to avoid smearing the interface between the fluid phases. All solution variables are stored at the cell centers of the Eulerian grid.

The octree grid is automatically generated and adaptively refined throughout the simulation. Boundary conditions from objects in the domain are treated with the mirroring immersed boundary method[18,19], in which the velocity field is implicitly mirrored across the boundary surface such that the given boundary condition is satisfied for the converged solution. No boundary-conforming mesh is required and arbitrary moving objects are handled with minimal manual user input.

The viscoelastic constitutive equation is solved in Lagrangian nodes, convected by the flow. For each Lagrangian node, Equation (4) is formulated in terms of the ordinary differential equation (ODE) systems

$$\dot{\mathbf{x}} = \mathbf{u}, \tag{9}$$

$$\dot{\tau} = G_k(\tau_k, \nabla\mathbf{u}), \quad k = 1,\ldots,N, \tag{10}$$

where $(\dot{\bullet})$ denotes time derivative and the right hand sides $G_1,\ldots,G_N$ follow directly from Equation (4) and (5).

The coupled ODE systems (9) and (10) are solved from time t to $t+\Delta t$ with a backwards-tracking procedure. At each node of the Eulerian fluid grid, one Lagrangian node is created. This is assumed to be the final location of the Lagrangian node, i.e. $\mathbf{x}|_{t+\Delta t}$. The initial location $\mathbf{x}|_t$, is calculated by integrating Equation (9) backwards in time. The corresponding stress τ_t is then interpolated to the node at $\mathbf{x}|_t$ and the system (10) is solved forward in time until $\tau|_{t+\Delta t}$ is obtained. When required, the fields $\mathbf{u}$ and $\nabla\mathbf{u}$ are interpolated from the Eulerian grid to the Lagrangian node. The solution procedure is visualized in Figure 1.

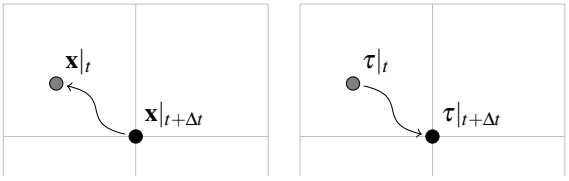

Figure 1. Backwards-tracking Lagrangian node position (left) and calculating viscoelastic stress (right).

When the stresses at time $t+\Delta t$ have been obtained, the values at the Eulerian cell centers are calculated from the values at the grid nodes. The viscoelastic contribution to the discretized momentum equation is then added as an explicit pseudo-force.

In the original Lagrangian-Eulerian method[28], Lagrangian nodes were initialized with a given distribution density, typically on the order of 4 nodes per cell, at the beginning of the simulation and the systems (9) and (10) were solved simultaneously. Unstructured interpolation using radial functions (RBF) was used to interpolate the viscoelastic stress to the Eulerian cell centers and nodes were added or deleted when required to maintain the quality of the node set, based on certain criteria.

In the new method, the need for unstructured interpolation as well as for adding or deleting nodes is eliminated. Furthermore, the total number of nodes is decreased. Hence, the method is more robust and the computational cost is reduced. As a reference, it was shown for the original Lagrangian-Eulerian method that approximately 30% of the stress calcula-

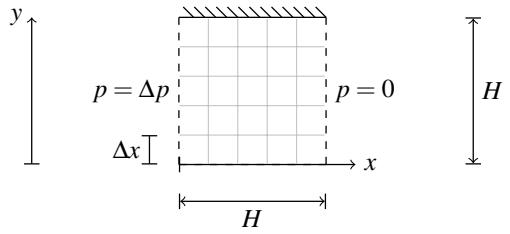

Figure 2. Schematic of the planar Poiseuille flow

tion time was spent on the unstructured interpolation and around 10% on the redistribution of Lagrangian nodes[29]. A detailed study of the computational efficiency is however outside the scope of this paper.

RESULTS

A planar Poiseuille flow is simulated with the proposed method. The flow geometry consists of a channel with height $2H$ and length H. Flow is initiated from rest by imposing a constant pressure drop Δp across the channel and periodic conditions are used for velocity and viscoelastic stress at the inlet and the outlet. At the upper wall the no-slip condition imposed and at the lower boundary a symmetry condition is used. Hence, half the channel is effectively simulated. A sketch of the geometry is shown in Figure 2.

The viscoelastic fluid is modeled as a single-mode Upper-Convected Maxwell (UCM) model, which is obtained by letting $\varepsilon = 0$ in Equation (4) and by using solvent viscosity $\mu = 0$ in the momentum equation. The Weissenberg number for the flow is defined as $Wi = U\lambda/H$, where U is the mean steady velocity. The flow is simulated for $Wi = 0.1, 1, 10$ with five uniform grids with spacing Δx such that $H/\Delta x = 5, 10, 20, 40, 80$.

The transient flow is simulated until steady state is reached. To achieve this in shorter calculation time and to improve numerical stability given the limiting case of $\mu = 0$, both sides diffusion with artificial viscosity $\mu_a = 10^2, 10^3, 10^4\,\mathrm{Pa\cdot s}$, respectively for $Wi = 0.1, 1, 10$, is used. It is remarked that this is feasible since only the steady solution is subject to analysis. The time steps used satisfy $\Delta t/\lambda = 10^{-4}$.

To validate the solution, the errors compared to the analytic solution are calculated as

$$E_\phi = \frac{||\phi_{\text{simulation}} - \phi_{\text{analytic}}||}{||\phi_{\text{analytic}}||}, \tag{11}$$

where $||\bullet||$ denotes the L_2 norm taken over the cells of the Eulerian grid and ϕ is either velocity or stress. The calculated errors for the streamwise velocity and the viscoelastic normal stress are shown in Figure 3. By calculating the slopes of the errors in log-space, it is found that the quantities converge to the analytic solution with second order accuracy, which is in agreement with previous work[28,29].

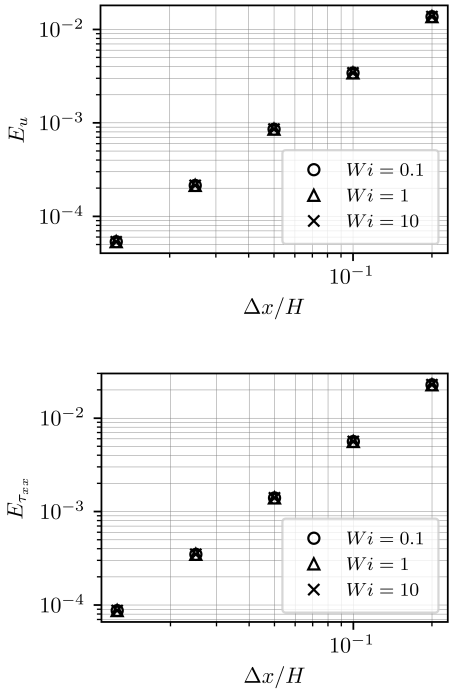

Figure 3. Computed errors compared to analytic solution for planar Poiseuille flow for velocity (top) and viscoelastic normal stress (bottom)

An industrial case of robot-carried application of a viscoelastic rubber adhesive on an automotive part is simulated. The circular nozzle has diameter 2 mm and moves along a predefined path. The adhesive flow rate is $0.736\,\mathrm{ml/s}$. An overview of the geometry and

the application path is shown in Figure 4. Furthermore, a 3D-scanned experimental adhesive bead for the case is available for comparison.

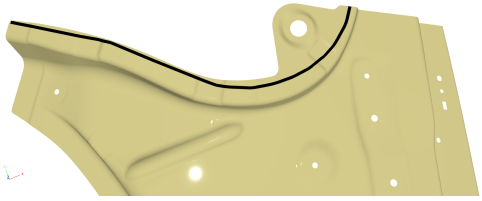

Figure 4. Overview of geometry and application path (black curve) moving from left to right in figure.

The adhesive is modeled with a six-mode PTT model fitted to available experimental data from small amplitude oscillatory shear (SAOS) experiments. The measurements were performed at RISE IVF in Mölndal, Sweden. Assuming small strain, the analytic expressions for the storage modulus G' and the loss modulus G'' read

$$G'(\omega) = \sum_{k=1}^{N} \frac{\eta_k \lambda_k \omega^2}{1+\lambda_k^2 \omega^2}, \tag{12}$$

$$G''(\omega) = \sum_{k=1}^{N} \frac{\eta_k \omega^2}{1+\lambda_k^2 \omega^2}, \tag{13}$$

where ω is the angular oscillation frequency. The parameters $\lambda_k, \eta_k, k = 1,\ldots,6$ are fitted using the GUSTL method by Kraus and Niederwald[25]. The results are shown in Figure 5 and the parameters are listed in Table 1. Measurement points at $\omega > 10^2$ have been excluded from the parameter fit to avoid influence of possible measurement artefacts at high frequencies. It is remarked that the wide range of relaxation times as well as the large polymeric viscosities puts high demand on the simulation framework in terms of numerical stability.

The value of ε_k is chosen to be 0.5 for all modes, which was found to give satisfying results. Furthermore, the solvent viscosity $\mu = 60\,\mathrm{Pa\cdot s}$ is used, estimated as the infinite shear

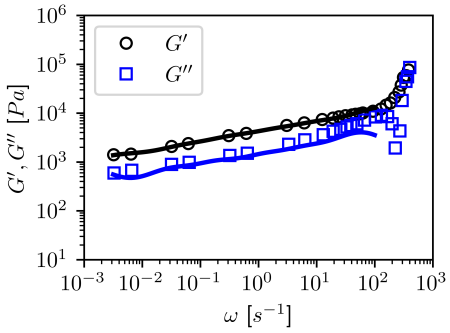

Figure 5. Viscoelastic modulii measured with SAOS (markers) and calculated with fitted model (solid lines).

k	λ_k [s]	η_k [Pas]
1	1000.0	$1.50\cdot10^6$
2	33.1	$3.16\cdot10^4$
3	5.06	6246
4	0.772	1202
5	0.149	317
6	0.0160	121

Table 1. Viscoelastic parameters for the PTT model used for the adhesive.

viscosity μ_∞ in the Carreau model, and the density of the adhesive is $2000\,\mathrm{kg/m^3}$.

The case features two-fluid flow of the applied adhesive and the surrounding air. Continuous inflow of adhesive into the domain is described by an injection model. In short, the grid is first refined around the nozzle. Injection cells are then identified and are filled with adhesive by modifying the local volume fraction α. The inlet velocity based on the volume flow rate is enforced through an immersed boundary condition.

Simulations are carried out for two grid resolutions. In both cases the coarsest cells consist of cubes with the side $\Delta x = 10\,\mathrm{mm}$. The grid is refined near the adhesive bead by recursively splitting the cells into eight smaller cells. The smallest cell sizes are $\Delta x_{\min} = 0.625\,\mathrm{mm}$ and $\Delta x_{\min} = 0.3125\,\mathrm{mm}$, respectively for the two simulations. The coarser simulation is carried out with a global time step $\Delta t = 5\cdot10^{-5}\,\mathrm{s}$ and the finer simulation with $\Delta t = 1\cdot10^{-5}\,\mathrm{s}$.

In Figure 6 a snapshot from the finer simulation is shown. The adhesive is visualized by the isosurface $\alpha = 0.5$, the injection cells as

solid cubes and the Lagrangian nodes are colored by the viscoelastic stress component τ_{zz}, where the injection is approximately in the z-direction.

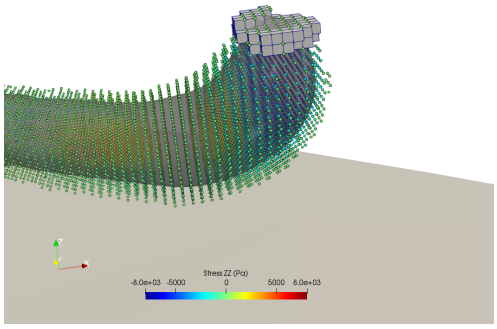

Figure 6. Snapshot of adhesive simulation.

In Figure 7 the simulated beads from the two simulations are compared to the 3D-scanned bead. The geometries of the simulated beads have been translated to enable the comparison. It is remarked that there may exist minor differences in the robot paths in the experiments and the simulation, particularly where the robot has to slow down due to reorientations. However, good overall agreement is found for both simulations. The scanned bead shows tendencies of fluid buckling, resulting in uneven features in the bead. This phenomenon may be difficult to predict through simulation. However, the fine simulation qualitatively predicts some degree of buckling.

A more detailed comparison between the simulations and the 3D-scan is made in the cross section in a part of the bead which is less affected by possible differences in the robot path. The location of the cross section is shown in Figure 8 and the comparison is shown in Figure 9. There are clear differences between the simulations and the scanned bead around the edges of the bead. However, these may be attributed to shadows in the scan. Considering this, the bead from the fine simulation is in excellent agreement with the scanned bead. The coarse one shows some discrepancies, but is in qualitative agreement with regards to the cross section geometry.

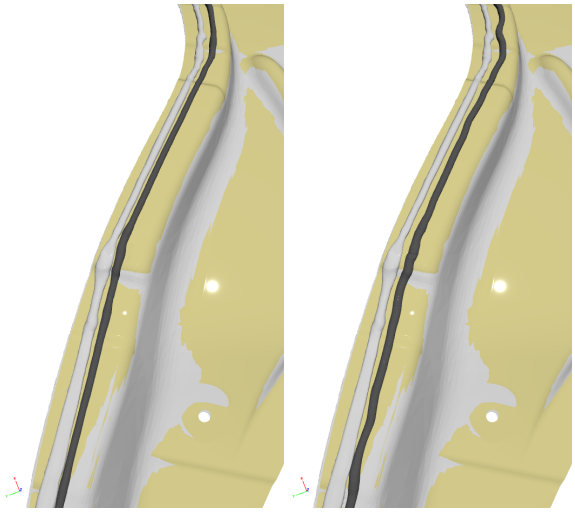

Figure 7. Comparison of simulated beads (dark gray) with $\Delta x_{\text{min}} = 0.625\,\text{mm}$ (left) and $\Delta x_{\text{min}} = 0.3125\,\text{mm}$ (right) and scanned bead (light gray).

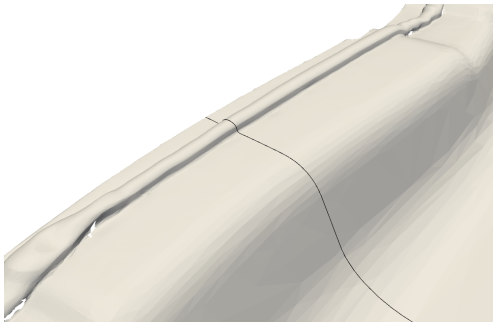

Figure 8. Cross section used for detailed comparison.

CONCLUSIONS

A numerical method for simulation of viscoelastic free-surface flow has been proposed. The new method is based on a previously developed Lagrangian-Eulerian framework for viscoelastic flow. The viscoelastic constitutive equation is solved in the Lagrangian frame of reference with a backwards-tracking procedure, while the remaining transport equations are solved with a Eulerian finite volume discretization. The discretization is performed on an automatic and adaptive octree grid and boundary conditions in the domain are treated using implicit immersed boundary conditions.

The new method improves the robustness

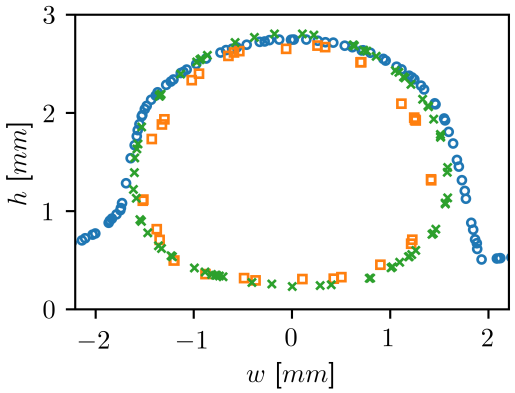

Figure 9. Detailed comparison of simulation with $\Delta x_{\text{min}} = 0.625\,\text{mm}$ (□), $0.3125\,\text{mm}$ (×) to 3D-scanned bead (○).

and computational efficiency compared to the original Lagrangian-Eulerian method. The accuracy of the method was validated for a viscoelastic planar Poiseuille flow as well as for an industrial scale case of adhesive application onto an automotive part. The results demonstrated that the proposed method produces results which are in good agreement with available analytic and experimental data. Furthermore, no additional stabilization technique was used for the adhesive simulation. Thus, given the large degree of elasticity of the adhesive, the simulations have shown that the proposed method is numerically robust.

ACKNOWLEDGEMENTS

This research has been partly carried out in a Centre for Additive Manufacturing – Metal (CAM2) in a joint project financed by Swedish Governmental Agency of Innovation Systems (Vinnova), coordinated by Chalmers University of Technology. The work has also been supported in part by Vinnova through the FFI Sustainable Production Technology program and in part by the Chalmers Area of Advance Production. The support is gratefully acknowledged. Scanned data and rheology measurements were obtained from RISE IVF.

REFERENCES

1. IPS IBOFlow, `http://ipsiboflow.com`.

2. Phan-Thien, N. (1978), "A Nonlinear Network Viscoelastic Model", *Journal of Rheology*, **22**, 259-283.

3. Doormaal, J. P. V. and Raithby, G. D. (1984), "Enhancements of the simple method for predicting incompressible fluid flows", *Numerical Heat Transfer*, **7**, 147-163.

4. Rasmussen, H. and Hassager, O. (1995), "Simulation of transient viscoelastic flow with second order time integration", *Journal of Non-Newtonian Fluid Mechanics*, **56**, 65 - 84.

5. Harlen, O., Rallison, J. and Szabo, P. (1995), "A split Lagrangian-Eulerian method for simulating transient viscoelastic flows", *Journal of Non-Newtonian Fluid Mechanics*, **60**, 81 - 104.

6. Baaijens, H. P., Peters, G. W., Baaijens, F. P. and Meijer, H. E. (1995), "Viscoelastic flow past a confined cylinder of a polyisobutylene solution", *Journal of Rheology*, **39**, 1243 - 1277.

7. Halin, P., Lielens, G., Keunings, R. and Legat, V. (1998), "The Lagrangian particle method for macroscopic and micro–macro viscoelastic flow computations Dedicated to Professor Marcel J. Crochet on the occasion of his 60th birthday.1", *Journal of Non-Newtonian Fluid Mechanics*, **79**, 387 - 403.

8. Oliveira, P., Pinho, F. and Pinto, G. (1998), "Numerical simulation of non-linear elastic flows with a general collocated finite-volume method", *Journal of Non-Newtonian Fluid Mechanics*, **79**, 1 - 43.

9. Gallez, X., Halin, P., Lielens, G., Keunings, R. and Legat, V. (1999), "The adaptive Lagrangian particle method for macroscopic and micro–macro computations of time-dependent viscoelastic flows", *Computer Methods in Applied Mechanics and Engineering*, **180**, 345 - 364.

10. Ubbink, O. and Issa, R. (1999), "A Method for Capturing Sharp Fluid Interfaces on Arbitrary Meshes", *Journal of Computational Physics*, **153**, 26 - 50.

11. Wapperom, P., Keunings, R. and Legat, V. (2000), "The backward-tracking Lagrangian

particle method for transient viscoelastic flows", *Journal of Non-Newtonian Fluid Mechanics*, **91**, 273 - 295.

12. Keunings, R. (2000), "A survey of computational rheology", in "Proceedings of the XII-Ith International Congress on Rheology",.

13. Alves, M., Pinho, F. and Oliveira, P. (2001), "The flow of viscoelastic fluids past a cylinder: finite-volume high-resolution methods", *Journal of Non-Newtonian Fluid Mechanics*, **97**, 207 - 232.

14. Alves, M. A., Oliveira, P. J. and Pinho, F. T. (2003), "Benchmark solutions for the flow of Oldroyd-B and PTT fluids in planar contractions", *Journal of Non-Newtonian Fluid Mechanics*, **110**, 45 - 75.

15. Fattal, R. and Kupferman, R. (2004), "Constitutive laws for the matrix-logarithm of the conformation tensor", *Journal of Non-Newtonian Fluid Mechanics*, **123**, 281 - 285.

16. Hulsen, M. A., Fattal, R. and Kupferman, R. (2005), "Flow of viscoelastic fluids past a cylinder at high Weissenberg number: Stabilized simulations using matrix logarithms", *Journal of Non-Newtonian Fluid Mechanics*, **127**, 27 - 39.

17. Fattal, R. and Kupferman, R. (2005), "Time-dependent simulation of viscoelastic flows at high Weissenberg number using the log-conformation representation", *Journal of Non-Newtonian Fluid Mechanics*, **126**, 23 - 37.

18. Mark, A. and Wachem, B. G. M. (2008), "Derivation and validation of a novel implicit second-order accurate immersed boundary method", *J. of Comput. Physics*, **227**, 6660 - 6680.

19. Mark, A., Rundqvist, R. and Edelvik, F. (2011), "Comparison Between Different Immersed Boundary Conditions for Simulation of Complex Fluid Flows", *Fluid dynamics & materials processing*, **7**, 241-258.

20. Balci, N., Thomases, B., Renardy, M. and Doering, C. R. (2011), "Symmetric factorization of the conformation tensor in viscoelastic fluid models", *Journal of Non-Newtonian Fluid Mechanics*, **166**, 546 - 553.

21. Mark, A., Svenning, E. and Edelvik, F. (2013), "An immersed boundary method for simulation of flow with heat transfer", *International Journal of Heat and Mass Transfer*, **56**, 424 - 435.

22. Mark, A., Bohlin, R., Segerdahl, D., Edelvik, F. and Carlson, J. S. (2014), "Optimisation of robotised sealing stations in paint shops by process simulation and automatic path planning", *International Journal of Manufacturing Research 5*, **9**, 4–26.

23. Svenning, E., Mark, A. and Edelvik, F. (2014), "Simulation of a highly elastic structure interacting with a two-phase flow", *Journal of Mathematics in Industry*, **4**, 7.

24. Svensson, M., Mark, A., Edelvik, F., Kressin, J., Bohlin, R., Segerdahl, D., Carlson, J. S. et al. (2016), "Process Simulation and Automatic Path Planning of Adhesive Joining", *Procedia CIRP*, **44**, 298 - 303.

25. Kraus, M. and Niederwald, M. (2017), "Generalized Collocation Method using Stiffness Matrices in the Context of the Theory of Linear Viscoelasticity (GUSTL)", *TECHNISCHE MECHANIK*, **37**, 82 - 106.

26. Edelvik, F., Mark, A., Karlsson, N., Johnson, T. and Carlson, J. (2017), "Math-Based Algorithms and Software for Virtual Product Realization Implemented in Automotive Paint Shops", 231-251.

27. Göhl, J., Markstedt, K., Mark, A., Håkansson, K., Gatenholm, P. and Edelvik, F. (2018), "Simulations of 3D bioprinting: predicting bioprintability of nanofibrillar inks", *Biofabriaction*, **10**,.

28. Ingelsten, S., Mark, A. and Edelvik, F. (2019), "A Lagrangian-Eulerian framework for simulation of transient viscoelastic fluid flow", *Journal of Non-Newtonian Fluid Mechanics*, **266**, 20 - 32.

29. Ingelsten, S., Mark, A., Jareteg, K., Kádár, R. and Edelvik, F. (2020), "Computationally efficient viscoelastic flow simulation using a Lagrangian-Eulerian method and GPU-acceleration", *Journal of Non-Newtonian Fluid Mechanics*, 104264.